Integrated out-of-plane nanoelectrospray thruster arrays for spacecraft propulsion

R Krpoun and H R Shea

Microsystems for Space Technologies Laboratory, School of Engineering, Ecole Polytechnique Fédérale de Lausanne, 2002 Neuchâtel, Switzerland

E-mail: renato.krpoun@a3.epfl.ch

Abstract

Nanoelectrosprays, well known for their use in sample injection for the mass spectrometry of large biomolecules, can also be used in other applications such as spacecraft propulsion. The thrust generated by a single electrospray emitter is well below 1 μN, which is several orders of magnitude below the required thrust for planned formation flying missions. This paper presents the process flow and the microfabrication of large 2D arrays of out-of-plane nanoelectrospray capillary emitters with integrated extractor electrodes as well as electrospray results. The capillaries, 70 μm high and with 24 μm inner diameter, are etched from one silicon-on-insulator wafer. The extractor electrodes are from another silicon-on-insulator wafer. Both parts are passively aligned to within 2 μm, centering each capillary under one extractor electrode, thus ensuring highly uniform emitter characteristics over large arrays. Low hydraulic impedance has been a major problem in out-of-plane electrospray designs in the past, which is solved here by adding a post-processing step in which the capillaries are filled with 5 μm silica microspheres fixed in place by silanization. Finally, this paper reports on successful spray tests carried out under vacuum conditions with single and arrays of capillaries spraying the ionic liquid EMI-Tf$_2$ N demonstrating the operation of our nanoelectrospray thrusters in an ionic mode.

(Some figures in this article are in colour only in the electronic version)

1. Introduction

The potential use of electrosprays for spacecraft propulsion was identified very early in the history of spaceflight [1], but only recent advances in electrospray technology, in particular the discovery of ionic liquids as fuels [2], have led to the development of a space qualified thruster [3]. Electrosprays have been popularized by their use in the field of mass spectrometry of large biomolecules [4]. Currently, other research areas include deposition of thin films [5] and femtoliter drops [6], electrospinning of nanofibers [7], small-scale combustion [8] and focused ion beam applications [9].

The principle of operation of an electrospray or colloid thruster consists of applying a potential difference between a conductive liquid inside a capillary (or at the tip of the needle) facing an annular extractor electrode. As the potential difference increases, the liquid at the tip sharpens and eventually, once a threshold voltage is reached, snaps into a cone-like protrusion, known as a Taylor cone [10],

and emission sets in. The emitted particles can be droplets, ions or a combination thereof. Figure 1 illustrates the arrangement for a capillary-type electrospray source. Figure 2 are micrographs illustrating the sharpening of the surface of the ionic liquid EMI-BF$_4$ at the tip of a 360 μm diameter silica capillary.

Planned formation flying missions, where several spacecraft fly at well-defined relative positions such as the joint ESA/NASA Laser Interferometer Space Antenna (LISA) project, require nanometer precision positioning of the satellites with respect to one another, which in turn requires a propulsion system offering thrust ranging from micro to milinewtons with a resolution below 0.1 μN and lifetimes larger than 10 000 h. Thrust, T, generated by an electrospray truster can be expressed as

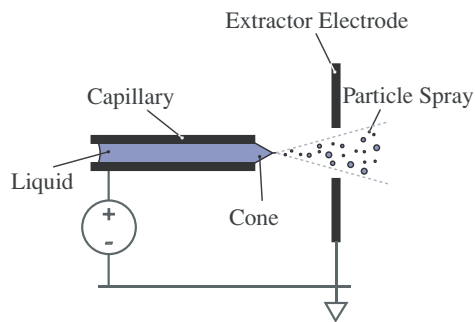$$T = I\sqrt{2\Phi_B \frac{m_0}{q}}, \qquad (1)$$

Figure 1. Schematic cross section of an electrospray or colloid thruster. Droplets and ions are extracted from a conductive liquid by applying a sufficiently large potential difference between the liquid and the extractor electrode.
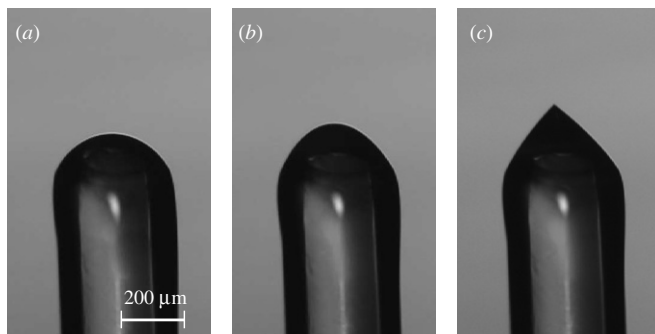

Figure 2. Sharpening of the surface of the ionic liquid EMI-BF$_4$ at the tip of a silica capillary with 360 μm diameter. The extractor electrode above the capillary is not visible in these micrographs. The voltages in this example are (*a*) 2.4 kV, (*b*) 2.6 kV and (*c*) 2.7 kV.

where I is the current, m_0 is the particle's mass, q is its charge, and Φ_B is the energy of the particle divided by its charge (beam potential) gained during its acceleration between the capillary and the extractor electrode. Due to energy losses in the ion or droplet extraction process, and a possible potential drop in the jet due to finite conductivity of the liquid, Φ_B, is lower than the capillary–ground potential difference by values ranging from a few volts to over hundred volts. Efficient propellant use (high specific impulse) requires a large q/m_0 ratio, yet thrust decreases with an increasing q/m_0 ratio, as seen from equation (1). Using arrays of emitters can allow both high thrust and high mass efficiency by operating in a high q/m_0 mode (ionic mode). Generally, for low-conductivity liquids (<0.8 S m^{-1}) charged droplets are emitted, and the electric current can be controlled by modulating the flow rate [11, 12] while for higher-conductivity liquids (>0.8 S m^{-1}) the current can be modulated by varying the applied voltage [13, 14]. For thruster applications, room-temperature ionic liquids are now the liquids on which new thruster designs are based. These liquids, having a non-measurable vapor pressure, are ideal for vacuum operation, and under the right conditions of flow rate and temperature allow the emission of a beam composed of ions (monomers, dimers) [2, 15–17].

Measurements have shown that the thrust of a single electrospray source is well below 1 μN [18–20]. To span the large thrust range required by future missions an array composed of thousands of emitters is needed.

Due to their purely electrostatic nature and the simple principle of operation, electrospray sources are good candidates for miniaturization, which allows us to significantly increase thrust density. Early work on single out-of-plane micromachined silicon emitters, without integrated extractor electrodes, has been done by Schultz *et al* [21] and Griss *et al* [22]. The latter developed a process flow to manufacture tapered tip capillaries; this design has served as a starting point for our capillary wafer process. Finally, one should also mention the high aspect ratio 1D arrays with silicon dioxide (SiO$_2$) capillaries having an inner diameter of 10 μm and 250 μm length without integrated electrodes reported by Wang *et al* [23].

One difficulty reported with out-of-plane emitters, i.e. structures perpendicular to the substrate, is the low hydraulic impedance between adjacent emitters leading to liquid spills and shorts between the extractor and emitter electrode [24]. This difficulty can be addressed by manufacturing in-plane thrusters [25] with long feed channels or by manufacturing porous silicon [26, 27] or tungsten needles [14]. The absence of precisely aligned extractor electrodes in these designs, in most cases a common 'macroscopic' electrode is used for all emitters, leads to inhomogeneities in spray properties between adjacent emitters which has a negative impact on thruster performance. One technique for aligning emitters and extractors was reported by Gassend *et al* [27] with a clip system allowing easy assembly and disassembly of the electrode; a major drawback of his system is the large surface area lost to the clip mechanism, and the added complexity and the relatively low precision which is around 10 μm.

We report here on the process flow and manufacturing results of a nanoelectrospray thruster with integrated extractor electrodes featuring an individual annular hole for each capillary emitter aligned to within 2 μm, ensuring highly uniform thrust and electrical characteristics over an array. The paper also presents lessons learned during microfabrication to obtain a high capillary yield and introduces a post-processing procedure to fill the capillary holes with silica microspheres allowing the hydraulic impedance of the individual emitters to be tailored both to control the operation mode of the capillary (ion or droplet) and preventing undesired liquid overflow. Finally, thruster operation under vacuum conditions for single and arrays of capillaries is demonstrated using the ionic liquid EMI-Tf$_2$N (also abbreviated as EMI-Im).

2. Thruster layout

The two main parts of the thruster are the microfabricated silicon capillaries and extractor electrodes. Figure 3 shows a schematic cross section across the thruster. The chip containing the capillaries is glued onto a low-temperature co-fired ceramic (LTCC) interface which provides the necessary high-voltage interfaces to power the thruster. On the opposite side of this glass–ceramic interface, a nanoport from Upchurch Scientific is mounted allowing us to attach a fused silica feed capillary, connecting the thruster to a fluid reservoir. Figure 4 shows the photograph of a fully assembled thruster. The picture also illustrates the mechanical interface made of PEEK
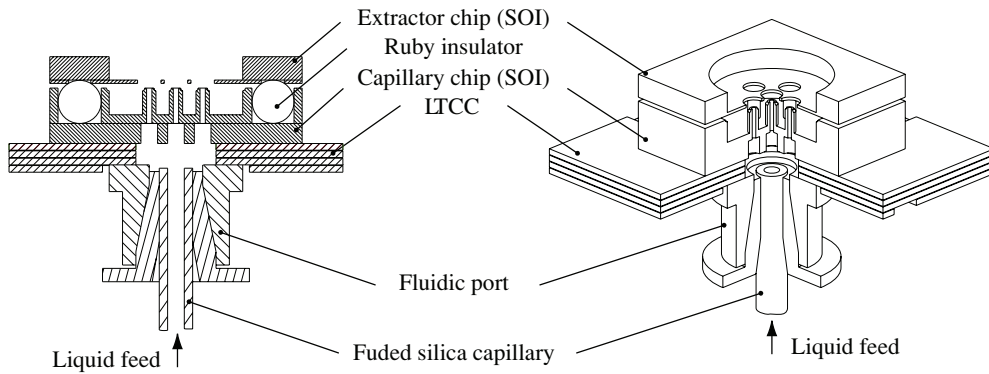
Figure 3. Nanoelectrospray thruster overview. Cross section of the thruster (not to scale). The core of the thruster is a microfabricated capillary chip and an extractor electrode both in silicon. The ruby balls serve as passive alignment features and also to insulate capillary and extractor electrode chips.
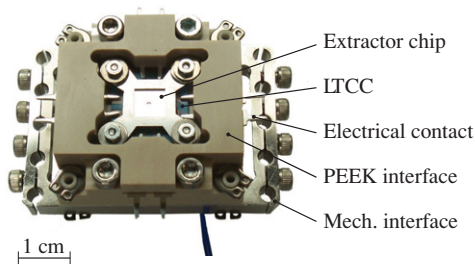

Figure 4. Photograph of the fully integrated thruster. The PEEK and stainless steel elements serve to mount the thruster to the holder in the vacuum chamber.

Figure 5. Photograph of the fully integrated thruster. The PEEK and stainless steel elements serve to mount the thruster to the holder in the vacuum chamber.

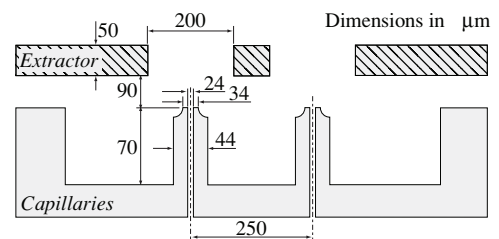and stainless steel which allows us to mechanically clamp the extractor electrode onto the capillary chip and acts as a mount to the holder in the vacuum chamber.

The thruster is assembled by first attaching the capillary chip and LTCC onto the PEEK and stainless steel support. Unlike a previous design [28] where the extractor electrodes were glued to the capillary chip, they can easily be disassembled in the present case. The advantage of this approach is the possibility of investigating failure modes after spray testing. Excellent alignment accuracy has been achieved by etching grooves on the four corners of the extractor electrode and capillary chips into which 200 μm diameter ruby balls can be placed. The ruby balls are placed manually into the groves, and assembly occurs by sliding the extractor electrode around until it 'snaps' into place. This method allows for an easy assembly process at the chip level and has led to highly reproducible results with alignment errors below 2 μm.

The dimensions of the microfabricated parts of the thruster are shown in figure 5, and have been optimized using a method allowing the calculation of the onset voltage and estimation of the crosstalk between capillaries [29]. The capillary stand-off height is 70 μm, and its inner diameter is 24 μm. This conservative aspect ratio has been chosen to allow good reproducibility of the capillaries during the manufacturing process and to achieve high yield. The capillary to extractor electrode distance is 90 μm with various extractor electrode hole diameter designs ranging from 150 μm up to 200 μm. The pitch between capillaries in the arrays is 250 μm.

3. Thruster fabrication

This section discusses the microfabrication process flow of the various elements of the thruster. It focuses mainly on the silicon micromachined parts (capillaries and extractor electrodes). The LTCC interface and assembly results are discussed in the second part of this section.

3.1. Capillary fabrication

The shape of the tip of the capillaries is based on an earlier design reported by Griss *et al* [22] which we altered in order to allow manufacturing of capillary arrays at the wafer scale. This design has been selected as the sharpening of the capillary toward the tip increases the electric field and thus decreases the operation voltage. Further a timed plasma etch on the backside of the capillaries has been validated introducing the capability to add fluidic channels on the backside of the chip. In the devices presented hereafter these fluidic structures serve solely to aid wetting of the capillaries, but adding channels in future designs and closing them by anodic bonding a Pyrex wafer will enable the integration of additional functionalities such as a feed system or liquid pumping into a small package. Further a post-processing step in which the capillaries are filled with silica beads allows matching the flow impedance to the needs of the final application.

The fabrication process, shown in figure 6, starts with the steam oxidation of a silicon-on-insulator (SOI) wafer with a 100 μm device layer, 1 μm buried oxide (BOX) and a
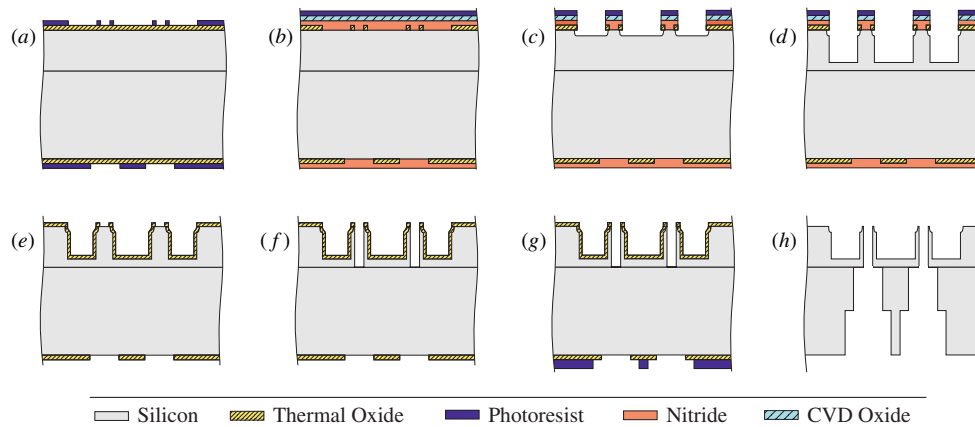
Figure 6. Illustration of the process flow developed to manufacture large arrays of capillary emitters. The process details are outlined in the text.

500 μm handle layer. After photolithography using AZ1518 photoresist (*a*) the exposed regions of the 1.5 μm thick oxide are removed in a buffered HF solution. This oxide layer defines the standoff structures which will protect the capillaries. Next, a thin 70 nm buffer thermal oxide is grown (not shown in the figure) acting as stress relief for a subsequent 150 nm LPCVD nitride layer. The latter serves as local protection of the silicon during steam oxidation. Finally, an additional 1 μm non-doped CVD oxide is deposited that serves as a hard mask (*b*). This oxide–nitride–oxide structure is patterned by reactive ion etching using an AZ1518 photoresist layer as a mask. The following isotropic RIE (*c*) and DRIE [30] yield the characteristic outer shape of the capillaries (*d*). After photoresist stripping and CVD oxide removal the wafers are once again steam oxidized. The resulting 1.5 μm thick oxide serves as a mask during the second DRIE which is performed once the nitride has been removed in a phosphoric acid bath (*e*). The second DRIE etches the inner hole of the capillaries (*f*). Once micromachining of the front side is accomplished the backside of the wafer is machined using a 'timed etch'. The silicon surface covered by a combined oxide–photoresist mask (AZ4562) is protected during the whole DRIE while the parts only covered by SiO$_2$ undergo a delayed etch. This delayed etch of silicon creates a structure with two different heights during one process step, which forms in our case the fluidic structures. Finally, the buried oxide is removed by means of a HF vapor etch [31] (h). Optionally the whole wafer can be oxidized to improve wetting properties and to change the electric field behavior at the tip of the capillary. A SEM photograph of a capillary cross section is shown in figure 7(*a*); the structures on the backside of the chip resulting from the timed etch serve to improve wetting, thus simplifying capillary filling is shown in figure 7(*b*).

Lift-up of the nitride during the second thermal oxidation, figure 6(*e*), has been observed causing oxidation of the capillary tip and leading to an important decrease in device yield. To avoid this defect we protect the tip with a silicon dioxide ring, shown schematically in figure 8. During the second oxidation step, this SiO$_2$ ring is pushed up by the growing oxide and a part of it eventually cracks and breaks away. To avoid lift-up of the entire protective SiO$_2$ ring and hence to avoid oxidation of the tip, the surface onto which the ring is attached on the needs to be sufficiently large (around 4.5 μm in our case).

To increase the hydraulic impedance silica microspheres are introduced into the capillaries by placing a drop of microspheres dispersed in a water/isopropyl solution on the back of the capillary chip. This solution is passively pulled into the capillaries through capillarity. Once dried, the microspheres are fixed together through a silanization process using silicon tetrachloride. The following reaction occurs:
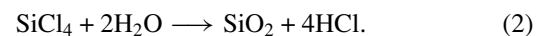
$$SiCl_4 + 2H_2O \longrightarrow SiO_2 + 4HCl. \tag{2}$$

Figure 7(*c*) is a micrograph of the resulting stack of microspheres inside the capillaries; in this experiment the microspheres are from Bangs Laboratories (Fishers, USA) and have a mean diameter of 4.74 μm. Tests to fill the capillaries with 1 μm beads were equally successful.

3.2. Extractor electrode fabrication

The extractor electrodes have been designed to match their capillary counterpart. Each capillary has an individual extractor hole, but electrically the whole extractor grid is addressed simultaneously. Fabrication starts once again with a SOI wafer (50/2/400) and an oxidation step (1.5 μm); figure 9(*a*). Alignment marks are then transferred into silicon dioxide on the handle layer side of the wafer using a buffered HF bath (*b*). The same procedure is then repeated on the device layer (*c*) followed by a DRIE up to the buried oxide (*d*). The wafer is turned and the handle layer is etched up to the buried oxide with a second DRIE using a thick AZ4562 photoresist mask (*e*). The buried oxide is removed from the handle layer side by vapor etching (*f*) and metalized with a layer of aluminum to decrease contact resistance (*g*).

3.3. LTCC

When the thruster is integrated into the satellite it will be exposed to the harsh space environment. Due to large temperature swings, such as those encountered when moving
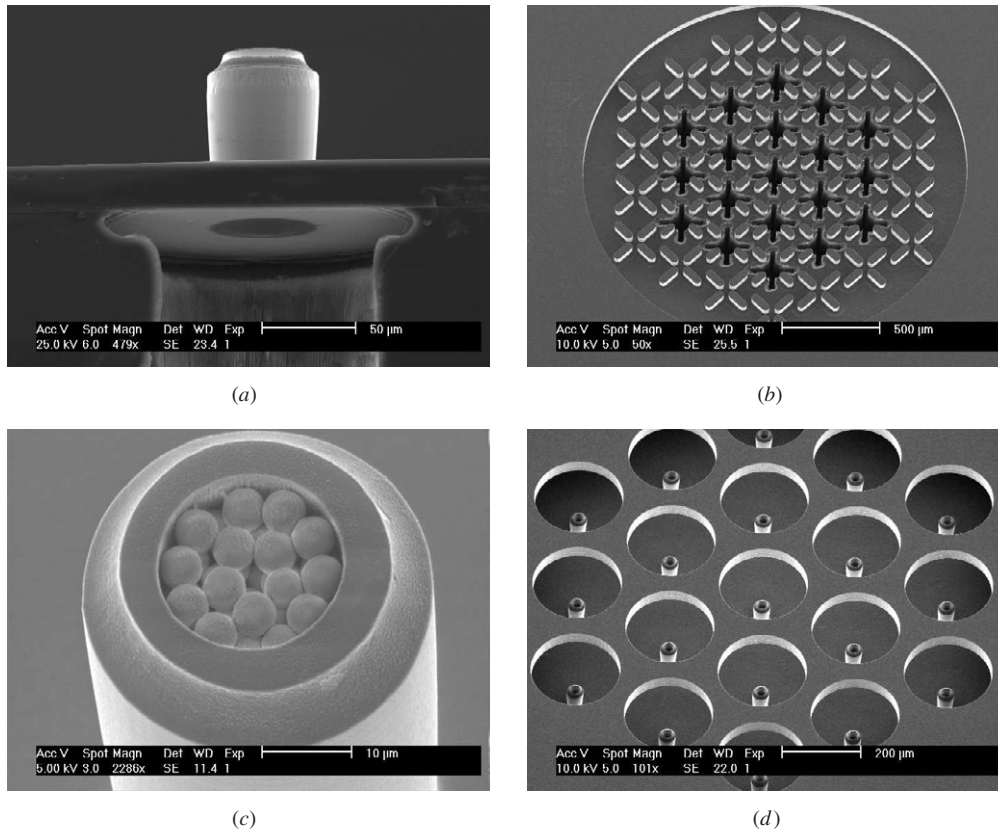
Figure 7. SEM photographs of the microfabricated parts of the thruster: (*a*) capillary cross section; notching at the buried oxide can be clearly seen, (*b*) structures on the backside of the capillary enhancing the wetting properties, (*c*) detail of the tip of a capillary filled with 5 μm silica beads, (*d*) assembled thruster array with an extractor electrode chip integrated onto the capillary chip.
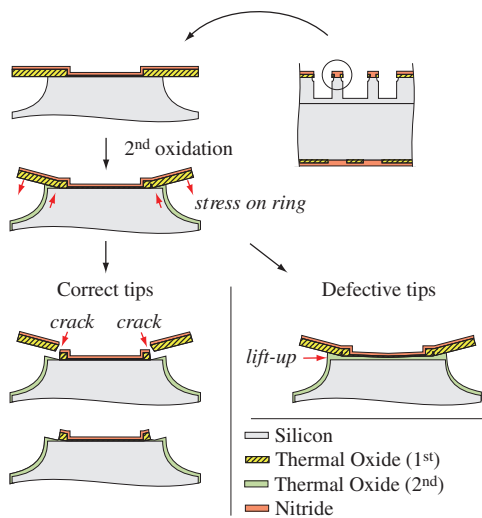

Figure 8. Illustration of the break up of the nitride–silicon dioxide ring. If the surface of the SiO$_2$ ring protecting the capillary tip is too small, the ring is lifted up and oxidation occurs below the nitride layer.

rapidly from daylight to eclipse, an active control of the thruster's temperature to prevent freezing of the fuel or a drift of thruster performance will be needed. To integrate a heater, thermal sensors, high-voltage electric connections and fluid interfaces into a miniaturized package a packaging technology known as low-temperature co-fired ceramic was chosen [32]. This technology consists in stacking sheets of glass–ceramic tapes, each containing structural or electric features, into a three-dimensional structure. After pressing this stack together, the laminated structure is sintered in an air furnace at 850–900 °C.

The features on each LTCC sheet may include holes, capacitors, resistors, electrical connections or vias. Holes are either drilled by laser or mechanical punching. Electrical traces and resistors are deposited through screen printing of different pastes. The LTCC sheets have a heat conductivity of 3.3 W m^{-1} K^{-1}, a density of 3.1 g cm^{-3} and a breakdown voltage of 1 kV/25 μm, and are therefore well adapted to high-voltage operation.

The developed prototype package consists of five ceramic sheets and includes an interface for an Upchurch Scientific nanoport, a network of positive temperature coefficient (PTC) resistors (for device heating and temperature measurement) and a fuel presence sensor. The PTC resistors have been integrated to heat the emitters and measure their temperature. They have been applied onto a ceramic sheet by screen printing and are, once the ceramics have been stacked and sintered, buried within the device and thus electrically separated from the fuel and the chip. In addition, a fill detector has also been included to measure the fill status of the thruster.
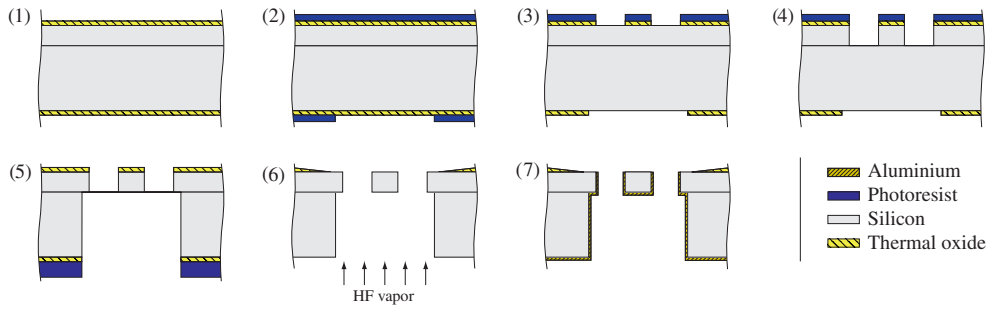
Figure 9. Manufacturing process flow of the extractor electrode. The process details are outlined in the text.
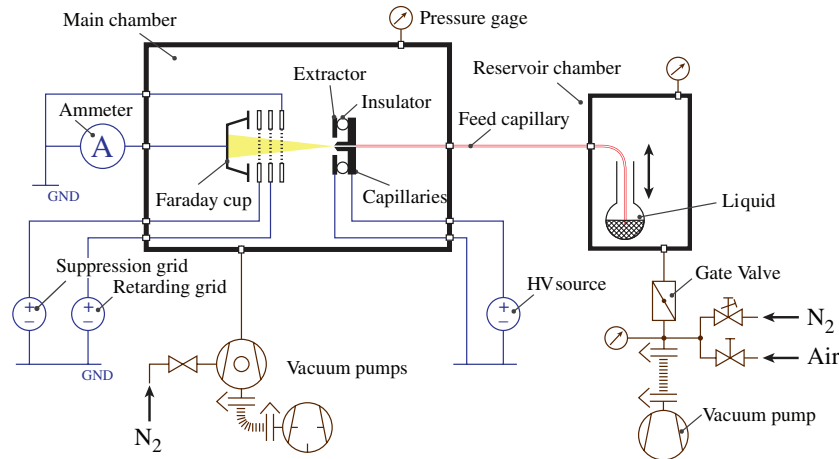

Figure 10. Schematic of the test setup for thruster characterization. The main chamber into which the thruster is mounted allows the characterization of the beam current by means of a Faraday cup and retarding potential analysis. The second vacuum chamber contains the liquid reservoir and can be pressurized. The liquid is pumped from the reservoir to the thruster through a 150 μm inner diameter silica capillary.

3.4. Assembly

Assembly starts by gluing the capillary chip onto the LTCC interface. This subassembly is then clamped between a macroscopic PEEK interface shown in figure 4. The extractor electrode chip is then integrated using 200 μm diameter ruby balls which insulate the extractor from the capillaries and serve also as passive alignment features providing an axial alignment error below 2 μm. Integration is accomplished by clamping down the extractor electrode using a stainless steel frame and mounting the thruster into the vacuum test chamber. A SEM photograph of the fully assembled thruster is shown in figure 7(*d*).

4. Experimental details

The test bench is illustrated schematically in figure 10, and consists of a vacuum chamber for thrust performance characterization and a second vacuum chamber for fuel storage. The latter is necessary to degas the ionic liquid before filling the thruster and thus to avoid bubble formation due to the water vapor and other contaminants present in the ionic liquid. Both chambers are connected through a fused silica feed capillary to transfer the liquid from the reservoir to the thruster. The main chamber used for thruster characterization consists of a six-way cross onto which a turbomolecular pump

(Varian Turbo-V 551, 550l/s) is directly attached through an ISO 160 interface. The base pressure attained in the main chamber is below 3×10^{-7} mbar and in the fluid reservoir below 5×10^{-3} mbar.

For spray testing the emitter capillaries are connected to the high-voltage source. As recommended by Lozano and Martínez-Sánchez [33] the polarity is switched periodically to avoid electrochemical reactions. During all tests the extractor electrodes are grounded and the emitter capillaries biased to high voltage. The electrospray current is measured by means of a Faraday cup (Kimball Physics FC-72A) attached to a picoammeter (Keithley 487). A grid placed in front of the Faraday cup and biased to −50 V suppresses secondary electrons. To analyze the energy spread of the beam, a retarding potential grid is placed in the beam path. As high-voltage sources, two Stanford Research Systems (PS350, ±5 kV) and a FuG Elektronik (HCN 35-6 500, ±6.5 kV) power sources are used.

The liquid feed system consists of a reservoir placed in a separate vacuum chamber connected to the main chamber through a silica capillary (360 μm o.d., 150 μm i.d.). The setup allows the operator to lower the feed capillary into the reservoir by means of a linear motion feedthrough. For long-term testing a gate valve allows sealing off the reservoir from the vacuum pump. To pressurize the reservoir and push the liquid through the capillary into the thruster a nitrogen purge
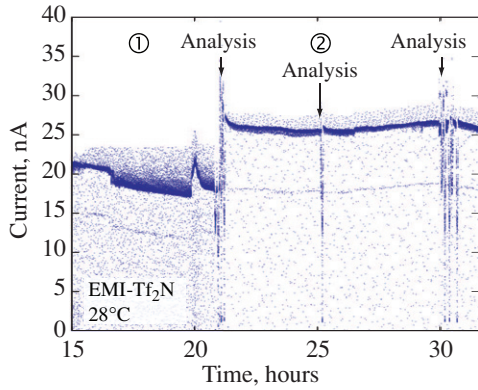
Figure 11. Current intensity measured at the Faraday cup between 15 and 33 h of the long-term test. The test was done with a single emitter capillary filled with microspheres. For clarity only the positive part of the current is shown. Two regions are marked indicating different regimes of operation. The emitter voltage was ±1000 V in region 1 and ±1200 V in region 2. The arrows labeled analysis correspond to retarding potential measurements.

valve with gradual control is installed. Pressure within the system is monitored by three Bayert-Alpert Pirani combination gages (Inficon BPG400).

5. Results and discussion

Tests were carried out successfully with single and arrays of capillaries spraying the ionic liquid 1-ethyl-3-methylimidazolium bis(trifluoromethylsulfonyl)imide (commonly referred to as EMI-Tf$_2$ N or EMI-Im). We report on a long-term test carried out over 64 h with a single capillary filled with 5 μm diameter silica microspheres with an integrated extractor electrode of 200 μm diameter placed 90 μm from the capillary tip. Additional details can be found in [34]. Figure 11 shows the current intensity recorded at the Faraday cup between 15 and 33 h acquired at a rate of 3 Hz. During this test, the voltage was switched at a rate of 0.25 Hz; in figure 11 only the positive current is shown for clarity. The numbered regions correspond to two emitter voltages: ±1000 V for region 1 (up to $t = 21$ h) and ±1200 V for region 2 (after $t = 21$ h).

Figure 12(*a*) shows the 'raw' current captured by the Faraday cup in region 1 for an emitter voltage of ±1000 V. There is a 150 ms delay between when the voltage is applied, and when spraying begins, for both polarities. In this case, the emitter voltage is set below the onset voltage of 1160 V computed using the model described in [29]. We assume therefore that, as the liquid is pushed through the capillary, a droplet forms at its tip which deforms, once a critical volume is reached, into a Taylor cone and spraying initiates. As can be seen in figure 11, the mean current value in region 1 fluctuates. As no visual data are available the exact cause of these fluctuations cannot be explained with certainty, but we assume that cone instabilities (indicated by the overshoot) lead to the formation of droplets which deposit on the extractor electrode, thus constantly altering the value of the measured current. If droplets are present they are also deposited onto
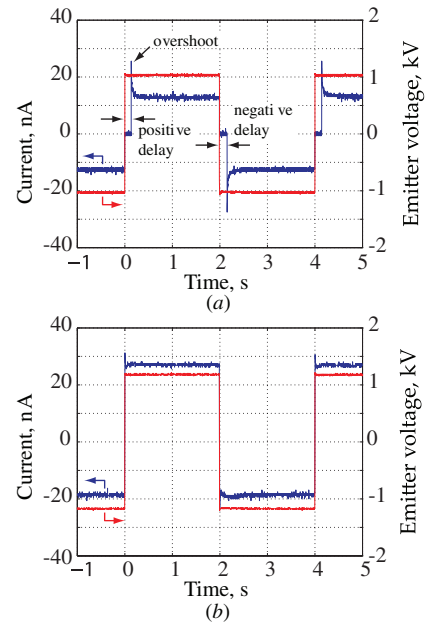

Figure 12. Measured current for a spray using the ionic liquid EMI-Tf$_2$ N as fuel. The polarity is periodically reversed to avoid electrochemical reactions. The trace (*a*) was recorded in region 1 and (*b*) in region 2 during the long-term test shown in figure 11.

the grid elements in front of the Faraday cup thus altering the current measurement. Increasing the voltage to ±1200 V leads to a stable spray current (region 2) shown in detail in figure 12(*b*). In this regime, the switching delay and overshoot disappear, and excellent spray stability is observed for several hours. Assuming operation in the ionic mode, as will be discussed hereafter, the increase in performance could be the result of high-speed ions slowly removing the deposited liquid on the extractor electrode and the grids.

In order to analyze the beam composition, the energy distribution of the beam has been studied by means of a retarding potential analyzer (RPA), which consists of a biased grid placed in front of the Faraday cup shown schematically in figure 10. This retarding potential grid acts as a barrier, only letting pass particles with a kinetic energy greater than the beam potential multiplied by the particle's charge:

$$\Phi_{RP} < \frac{1}{2}\frac{m_e}{q}\mathbf{u}_e^2, \tag{3}$$

where Φ_{RP} is the retarding potential, q/m_e is the charge over mass ratio of the particle, and $\mathbf{u}_e$ is its speed. Differentiating the measured particle current with respect to the retarding voltage yields the energy density distribution. The RPA used in our experiments consists of a single grid, which is not a perfect equipotential plane. Between grid wires the potential 'sags' which limits the resolution of the system [35]. In our case, we estimate the voltage between the two grid wires to be 5–10% below the applied grid voltage.

In region 2 of the long-duration test three current versus retarding potential traces were recorded at an emitter voltage of ±1200 V, marked as 'analysis' in figure 11 and shown in figure 13(*a*). The solid line is the interpolating spline used to compute the density distribution shown in figure 13(*b*). A
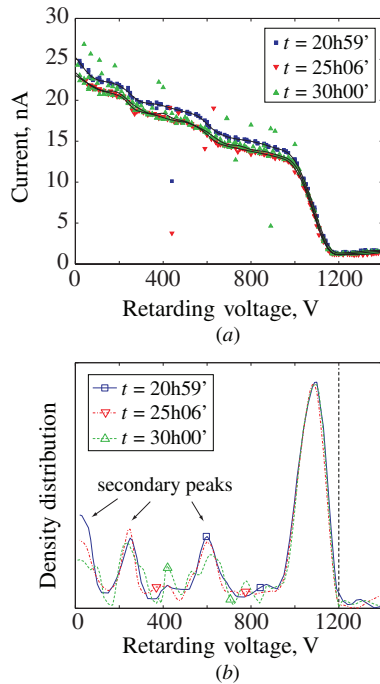
(a)

(b)

Figure 13. Retarding potential measurement of a beam emitted from a single capillary at 1.2 kV after 21, 25 and 30 h of spray testing. (*a*) Current versus retarding voltage, the solid line represents the interpolating spline. (*b*) Energy density distribution of the beam, indicating mostly ionic operation.

primary peak in the energy density is visible around a retarding potential grid voltage of 1100 V, indicating that most of the emitted ions or droplets have an energy very near $q V_{emitter}$, i.e., a small energy deficit, hence a very efficient emission process. As discussed in the previous paragraph, the single grid RPA has a limited resolution, in consequence the primary peak's voltage deficit could be less than 50 V from the voltage applied to the capillary. These results are very similar to traces recorded with the same ionic liquid by Lozano [36] using single, needle-type emitters without integrated extractor electrodes. With his test setup he could additionally measure the charge-over-mass ratio of the particles which showed a beam composed of the EMI^+ monomer and the $(EMI\text{-}Tf_2 N)EMI^+$ dimer. Lozano observed with a high-resolution RPA that in the ionic mode there is a very low energy deficit (in the order of 5 eV) and a narrow energy distribution (8 eV full width at half maximum). He attributes the secondary peaks to the fragmentation of solvated ions. On the other hand, Gamero-Castaño [37] observes an energy deficit of several hundreds eV for a beam operating in a mixed ion–droplet mode. Based on the similarities with the data recorded by Lozano, it is reasonable to conclude that our beam consists of ions rather than droplets.

　　For operation after 33 h the flow rate is decreased and a slow degradation of the stability of the spray current can be observed. This is attributed to increased damage of the extractor electrode. The SEM photograph of the extractor electrode (upstream side) after 64 h of testing is shown in figure 14(*b*). In addition to the sputtering of the electrode, which can be clearly seen, deposits were observed on both of its sides. It should be clearly noted that in this test several
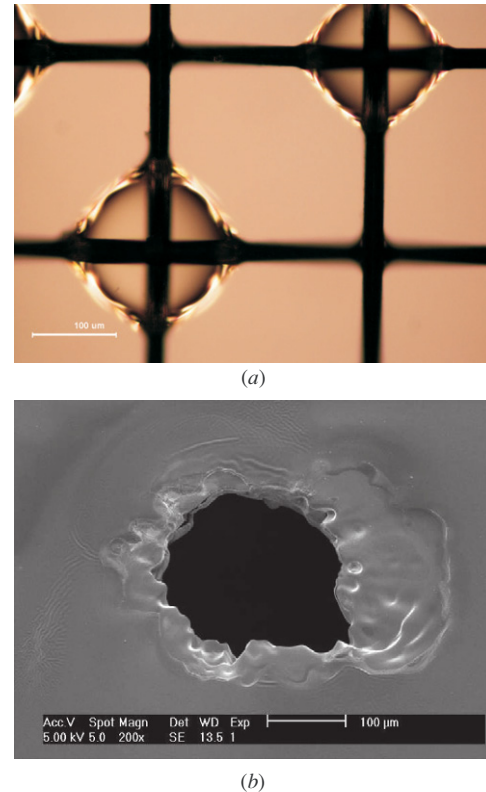

(a)

(b)

Figure 14. Component analysis after spray testing. (*a*) Micrograph of the grounded grid of the RPA. Deposition of ionic liquid agglomerating into droplets can be clearly seen. (*b*) Sputtering effect of the extractor electrode after 64 h of spraying on the upstream side observed on a SEM photograph.

operational modes were probed, some of which had a much stronger lifetime impact on the electrode, therefore at present only limited data are available on thruster lifetime; further tests at various voltage levels and test durations are required to identify regions of operation where extractor erosion is minimal and to make lifetime projections.

　　Assuming an ionic beam, the thrust for a single emitter (spraying in a positive mode) can be calculated using equation (1). The thrust generated by a single emitter is therefore 0.002 μN which is well below the required thrust resolution. Extrapolating this result to large arrays such as those present in figure 7(*d*) with a pitch of 250 μm between capillaries leads to an estimated thrust of 100 μN on a 5 × 5 cm^2 surface (manufacturable on a 4 inch wafer). By optimizing the geometry and by adding an acceleration electrode thrust density could be increased by at least one order of magnitude while keeping the thruster operating in the ionic mode (the present emitter density is larger than 1800 emitters cm^{-2}). Assuming a beam composed of monomers and dimers the specific impulse of this thruster can be calculated to lie between 2000 and 4600 s. Finally, the capability to tailor the flow impedance, i.e., matching the emitted flow with the supplied one, by adding microspheres could be used so that only certain parts of the thruster array spray in the droplet mode, thus decreasing the charge-over-mass ratio leading to a significant increase in thrust while keeping the same architecture. These 'low' hydraulic impedance sections of the
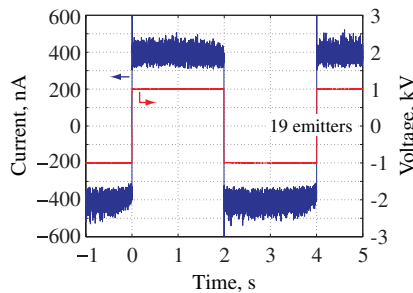
Figure 15. Electrospray data for a 19-emitter array filled with 5 μm diameter microbeads biased to ±1000 V. The layout is as illustrated in figure 7(*d*).

thruster could be activated when necessary and would further extend the thrust range of the system.

The electrospray current of a 19-emitter array with the same dimensions as the single emitter also filled with microspheres and spraying EMI-Tf$_2$ N at ±1000 V is shown in figure 15. Compared to a single emitter the overall current from the array is lower than expected. Observation of deposits on the grid and screen elements preceding the Faraday cup lead to the conclusion that, for an array, part of the beam current is not collected by the Faraday cup accounting for this current deficit.

6. Conclusion

We have demonstrated the feasibility of an electrospray thruster consisting of microfabricated out-of-plane capillary arrays with integrated extractor electrodes. The process flow we developed allows the fabrication of arrays of capillaries with high yield. To tailor the flow impedance of the capillaries a post-processing step has been developed in which the capillaries are filled with 5 μm diameter microspheres which are fixed inside the capillaries through a silanization process using SiCl$_4$. Chip scale assembly and insulation between the extractor electrodes and the capillaries is achieved using a passive alignment system which consists of 200 μm diameter ruby balls placed into grooves etched into both the capillary and extractor electrode chips.

Electrospray results obtained under vacuum conditions with the ionic liquid EMI-Tf$_2$ N have shown a stable spray for several hours. For this ionic liquid the energy density distribution corresponds to previous work on macrodevices and indicates an ionic beam. Future work will focus on the characterization of the various operation modes of the thruster as a function of parameters such as the voltage, mass flow rate and temperature. Research is also required on how to achieve the required thrust modulation ranging from micro to millinewton. One possible approach would be to integrate micropumps on the backside of the capillary wafer. In this approach, every micropump would feed a small segment of the thruster. The long-term goal is to reach a thruster lifetime of several thousand hours, as required by several planned spacecraft missions.

References

[1] Hendricks C D 1962 *J. Colloid Sci.* **17** 249–59
[2] Romero-Sanz I, Bocanegra R and Fernandez de la Mora J 2003 *J. Appl. Phys.* **94** 3599–605
[3] Ziemer J K, Randolph T M, Franklin G W, Hruby V, Spence D, Demmons N, Roy T, Ehrbar E and Zwahlen J 2008 *Proc. 44th AIAA/ASME/SAE/ASEE Joint Propulsion Conf. Exhibit (Hartford)* AIAA 2008-4826
[4] Fenn J, Mann M, Meng C, Wong S and Whitehouse C 1989 *Science* **246** 64–71
[5] Jaworek A 2007 *J. Mater. Sci.* **42** 266–97
[6] Paine M, Alexander M, Smith K, Wang M and Stark J 2007 *J. Aerosol Sci.* **38** 315–24
[7] Reneker D H, Yarin A L, Fong H and Koombhongse S 2000 *J. Appl. Phys.* **87** 4531–47
[8] Deng W, Klemic J, Li X, Reed M and Gomez A 2006 *J. Aerosol Sci.* **37** 696–714
[9] Zorzos A and Lozano P 2008 *Proc. 52nd Int Conf. on Electron, Ion, Photon Beam Technology and Nanofabrication (Portland, OR)* p 35910
[10] Taylor G 1964 *Proc. R. Soc.* A **280** 383–97
[11] Fernández de la Mora J and Loscertales I 1994 *J. Fluid Mech.* **260** 155–84
[12] Gañán Calvo A M 2004 *J. Fluid Mech.* **507** 203–12a
[13] Smith K L, Alexander M S and Stark J P W 2006 *J. Appl. Phys.* **99** 064909
[14] Legge R S and Lozano P 2008 *Proc. 44th AIAA/ASME/SAE/ASEE Joint Propulsion Conf. Exhibit (Hartford, CT)* AIAA 2008-5002
[15] Lozano P and Martínez-Sánchez M 2005 *J. Colloid Interface Sci.* **282** 415–21
[16] Castro S, Larriba C, De La Mora J, Lozano P, Sümer S, Yoshida Y and Saito G 2007 *J. Appl. Phys.* **102** 94310
[17] Garoz D, Bueno C, Larriba C, Castro S, Romero-Sanz I, De La Mora J, Yoshida Y and Saito G 2007 *J. Appl. Phys.* **102** 064913
[18] Stark J, Stevens B, Alexander M and Kent B 2005 *J. Spacecr. Rockets* **42** 628–39
[19] Ziemer J K, Gamero-Castaño M, Hruby V, Spence D, Demmons N, R M, Roy T, Gasdaska C, Young J and Connolly B 2005 *Proc. 41st AIAA/ASME/SAE/ASEE Joint Propulsion Conf. Exhibit (Tucson, AZ)* AIAA 2005-4265
[20] Guerreo I, Bocanegra R, Higuera F and Fernández De La Mora J 2007 *J. Fluid Mech.* **591** 437–59
[21] Schultz G A, Corso T N, Prosser S J and Zhang S 2000 *Anal. Chem.* **72** 4058–63
[22] Griss P, Melin J, Sjödahl J, Roeraade J and Stemme G 2002 *J. Micromech. Microeng.* **12** 682–7

[23] Wang L, Stevens R, Malik A, Rockett P, Paine M, Adkin P, Martyn S, Smith K, Stark J and Dobson P 2007 *Microelectron. Eng.* **84** 1190–3

[24] Paine M D, Gabriel S, Schabmueller C G J and Evans A G R 2004 *Sensors Actuators* A **114** 112–7

[25] Velásquez-García L 2004 The design, fabrication and testing of micro-fabricated linear and planar colloid thruster arrays *PhD Thesis* Massachusetts Institute of Technology (MIT)

[26] Velásquez-García L F, Akinwande A I and Martínez-Sánchez M 2006 *J. Microelectromech. Syst.* **15** 1272–80

[27] Gassend B, Velásquez-García L F, Akinwande A I and Martínez-Sánchez M 2008 *Proc. 21st IEEE Int. Conf. on Micro Electro Mechanical Systems (Tucson, AZ)* pp 976–9

[28] Krpoun R, Räber M and Shea H R 2008 *Proc. 21st IEEE Int. Conf. on Micro Electro Mechanical Systems (Tucson, AZ)* vol 0234 pp 964–7

[29] Krpoun R and Shea H R 2008 *J. Appl. Phys.* **104** 064511–8

[30] Laermer F and Shilp A 1994 Method of anisotropically etching silicon, Robert Bosch GmbH, *US Patent* 5501893

[31] Overstolz T, Clerc P, Noell W, Zickar M and De Rooij N 2004 *Proc. 17th IEEE Int. Conf. on Micro Electro Mechanical Systems (Maastricht)* pp 717–20

[32] Gongora-Rubio M R, Espinoza-Vallejos P, Sola-Laguna L and Santiago-Avilés J J 2001 *Sensors Actuators* A **89** 222–41

[33] Lozano P and Martínez-Sánchez M 2004 *J. Colloid Interface Sci.* **280** 149–54

[34] Krpoun R 2008 Micromachined electrospray thrusters for spacecraft propulsion *PhD Thesis* Ecole Polytechnique Fédérale de Lausanne, Switzerland

[35] Enloe C L and Shell J R 1992 *Rev. Sci. Instrum.* **63** 1788–91

[36] Lozano P 2006 *J. Phys. D: Appl. Phys.* **39** 126–34

[37] Gamero-Castaño M 2008 *Phys. Fluids* **20** 032103